AGU PUBLICATIONS

Geophysical Research Letters

RESEARCH LETTER
10.1002/2014GL060881

Key Points:
- Atmospheric rivers explain East Antarctic anomalous SMB in 2009 and 2011
- ARs link Antarctic snowfall and accumulation to subtropical moisture sources
- Recent extreme meridional moisture fluxes to DML stand out in a long-term record

Correspondence to:
I. V. Gorodetskaya,
Irina.Gorodetskaya@ees.kuleuven.be

Citation:
Gorodetskaya, I. V., M. Tsukernik, K. Claes, M. F. Ralph, W. D. Neff, and N. P. M. Van Lipzig (2014), The role of atmospheric rivers in anomalous snow accumulation in East Antarctica, *Geophys. Res. Lett.*, *41*, 6199–6206, doi:10.1002/2014GL060881.

Received 11 JUN 2014
Accepted 8 AUG 2014
Accepted article online 14 AUG 2014
Published online 15 SEP 2014

The role of atmospheric rivers in anomalous snow accumulation in East Antarctica

Irina V. Gorodetskaya[1], Maria Tsukernik[2], Kim Claes[1], Martin F. Ralph[3], William D. Neff[4,5], and Nicole P. M. Van Lipzig[1]

[1]Department of Earth and Environmental Sciences, KU Leuven - University of Leuven, Leuven, Belgium, [2]Environmental Change Initiative, Brown University, Providence, Rhode Island, USA, [3]Center for Western Weather and Water Extremes, University of California, San Diego, La Jolla, California, USA, [4]Earth System Research Laboratory, NOAA, Boulder, Colorado, USA, [5]Cooperative Institute for Research in the Environmental Sciences, University of Colorado Boulder, Boulder, Colorado, USA

Abstract Recent, heavy snow accumulation events over Dronning Maud Land (DML), East Antarctica, contributed significantly to the Antarctic ice sheet surface mass balance (SMB). Here we combine in situ accumulation measurements and radar-derived snowfall rates from Princess Elisabeth station (PE), located in the DML escarpment zone, along with the European Centre for Medium-range Weather Forecasts Interim reanalysis to investigate moisture transport patterns responsible for these events. In particular, two high-accumulation events in May 2009 and February 2011 showed an atmospheric river (AR) signature with enhanced integrated water vapor (IWV), concentrated in narrow long bands stretching from subtropical latitudes to the East Antarctic coast. Adapting IWV-based AR threshold criteria for Antarctica (by accounting for the much colder and drier environment), we find that it was four and five ARs reaching the coastal DML that contributed 74–80% of the outstanding SMB during 2009 and 2011 at PE. Therefore, accounting for ARs is crucial for understanding East Antarctic SMB.

1. Introduction

A small number of high snow accumulation events over the Antarctic ice sheet related to intense snowfall can contribute significantly to local surface mass balance (SMB), both over the ice sheet interior and over the escarpment and coastal areas [*Braaten*, 2000; *Fujita et al.*, 2011; *Gorodetskaya et al.*, 2013; *Noone et al.*, 1999; *Schlosser et al.*, 2010]. For example, a few strong snowfall events over Dronning Maud Land (DML) in 2009 and 2011 produced a positive mass anomaly over the East Antarctic ice sheet, counterbalancing the increasing ice discharge from West Antarctica in these years [*Boening et al.*, 2012; *King et al.*, 2012; *Shepherd et al.*, 2012; *Rignot et al.*, 2014; *McMillan et al.*, 2014]. Using regional climate model output and accumulation records from firn cores, *Lenaerts et al.* [2013] showed that the 2009 and 2011 extreme snowfall and SMB anomalies in East Antarctica were unprecedented in the last 60 years, and only a few other similarly large SMB anomalies occurred since the mideighteenth century.

Synoptic activity over the Southern Ocean plays an important role in delivering precipitation to the Antarctic continent, both to the coastal areas and, as many recent studies suggest, further inland [*Bromwich*, 1988; *Braaten*, 2000; *Fujita et al.*, 2011; *Hirasawa et al.*, 2000, 2013; *Reijmer and van den Broeke*, 2003; *Schlosser et al.*, 2010; *Noone et al.*, 1999; *Tsukernik and Lynch*, 2013]. Furthermore, synoptic-scale snowfall events of large magnitude require significant poleward moisture transport. In midlatitudes the majority of moisture transport is organized in narrow and long band features known as "atmospheric rivers" (ARs) [*Zhu and Newell*, 1998; *Ralph et al.*, 2004]. The importance of ARs for the coastal precipitation in midlatitudes is tremendous: in California they can result in severe rainfall events causing floods [*Ralph et al.*, 2006, 2014; *Bao et al.*, 2006] contributing strongly to the state's total annual precipitation [*Dettinger et al.*, 2011], and in the South American Andes they are responsible for most of the heavy winter orographic precipitation events [*Viale and Nuñez*, 2011]. *Lavers et al.* [2011] and *Lavers and Villarini* [2013] linked AR events to recent flooding and extreme precipitation in Europe. An AR transporting large amounts of warm and humid air generated by the North American heat wave and subsequent evaporation from the ocean was one of the important factors behind the anomalous melt event over the Greenland ice sheet in July 2012 [*Neff et al.*, 2014]. ARs can provide an important linkage between tropical moisture sources and extratropical precipitation in both

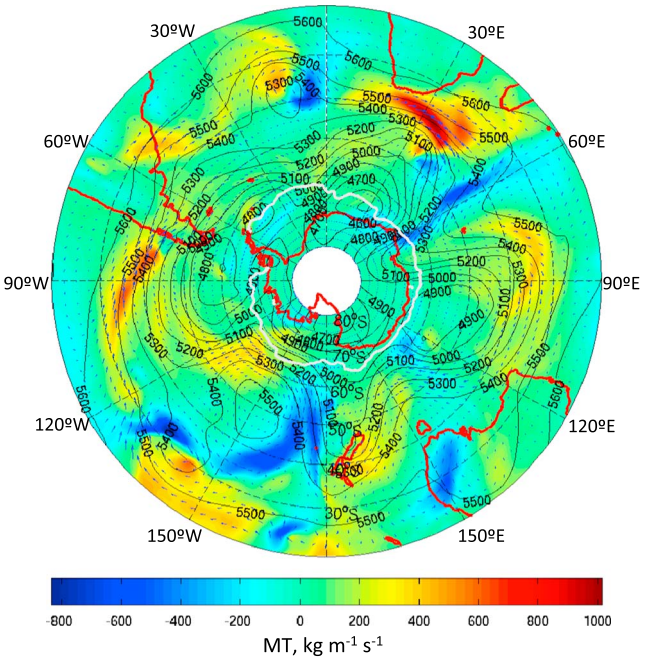

Figure 1. Vertically integrated total moisture transport (MT, kg m^{-1} s^{-1}; equation (3), colors and arrows) and 500 hPa geopotential heights (meters, contours) for 20°S–80°S on 19 May 2009, 00 UTC. Positive MT indicates north and eastward directions, negative MT indicates south and westward directions. Gray line shows the daily mean sea ice boundary at 20% threshold. Thick red lines show continental contours. Based on the ERA-I reanalysis data.

hemispheres [*Bao et al.*, 2006; *Ralph et al.*, 2011; *Knippertz et al.*, 2013]. Figure 1 illustrates moisture transport patterns over the Southern Hemisphere on one particular day (19 May 2009), clearly showing several narrow bands, where moisture fluxes are tens to hundreds of times greater than the mean field.

Here we analyze for the first time the impact of AR's on the East Antarctic precipitation and accumulation, using in situ measurements of snow accumulation and radar-derived snowfall estimates from Princess Elisabeth station (PE) located in the escarpment area of DML (71°57′S, 23°21′E, 1.4 km above sea level, 173 km from the coast). Combining in situ measurements with the European Centre for Medium-range Weather Forecasts (ECMWF) Interim (ERA-I) reanalysis data [*Dee et al.*, 2011], we examine moisture transport patterns that produce high-accumulation events. After detailed analysis of two particularly high accumulation cases that involved ARs, we investigate the role of ARs in other high-accumulation events during the 4 year period (2009–2012) covered by accumulation measurements at PE. Further, we evaluate moisture transport into the East Antarctica in a broader temporal and spatial context and confirm that the anomalous moisture transport in 2009 and 2011 resulted from its extreme meridional nature.

2. Data and Methods

Snow accumulation during 2009–2012 is calculated based on hourly snow height measurements using an acoustic depth gauge installed as part of an automatic weather station (AWS) 300 m east from PE during 2 February 2009 to 31 December 2012 [*Gorodetskaya et al.*, 2013, 2014]. Snow height measurements are converted to water equivalent (w.e.) using snow density measurements performed every summer near the AWS [*Gorodetskaya et al.*, 2013]. Daily mean accumulation is calculated as the difference between daily mean cumulative snow height changes between each pair of consecutive days. High-accumulation events are identified if daily accumulation exceeds 10 mm w.e., which is the 95th percentile (commonly used to characterize extreme precipitation, e.g., *Kopparla et al.* [2013] and *Viale and Nuñez* [2011]) based on 2009–2012 daily mean positive accumulation values.

Large-scale circulation and moisture transport patterns are investigated using the ERA-I data at 79 km horizontal resolution further interpolated on 0.25° × 0.25° horizontal grid. The tropospheric layer of 900–300 hPa is used for the analysis as the layer containing the majority of the poleward moisture flux reaching the Antarctic grounding line (i.e., coastline excluding ice shelves [*Van Lipzig and van den Broeke*, 2002]). We chose not to include the layer between the surface and 900 hPa to avoid contamination of the signal by the katabatic flow directed equatorward, which is very prominent near the edge of the continent [e.g., *Van Lipzig and van den Broeke*, 2002; *Tsukernik and Lynch*, 2013]. ERA-I shows the best performance compared to other reanalysis products in simulating main characteristics of ARs in midlatitudes [*Wick et al.*, 2013], as well as Antarctic precipitable water and precipitation [*Nicolas and Bromwich*, 2011].

Table 1. Mean Daily Snow Accumulation (Acc) Amount and Snowfall Rates (*S*) for Each High-Accumulation Event at PE Associated With ARs, From 2 February 2009 to 31 December 2012[a]

Year and Dates of High Acc Events With AR	*Contribution to Annual Acc, %; Acc* Each Event, (mm w.e. d^{-1})	*S* Each Event (mm w.e. d^{-1})	Date AR Detected	AR Coastal Longitude
2009	*74%*			
18 and 19 May	25	N/A	18 and 19 May	59°E
25 May	24	N/A	25 May	10°E
15 and 16 Jun	23	N/A	16 Jun	52°E
5 and 6 Jul	24	N/A	6 and 7 Jul	40°E, 45°E
2010	*No AR Events*			
2011	*80%*			
14–16 Feb	24	14–25	15 Feb	30°E
24 Jun	30	N/A	24 Jun	15°E
20 and 21 Nov	13	N/A	22 Nov	58°E
15–17 Dec	14	16–30	16 Dec	32°E
19 and 20 Dec	20	3–5	19 Dec	60°E
2012	*46%*			
6 Nov	24	9–15	5 and 6 Nov	7°E

[a]Snowfall rate is given as a range based on Z_e-*S* relationships for dry snow according to *Matrosov* [2007] (see section 2). Contribution of all events to the annual accumulation (%) is given in italics for each year. AR coastal longitude indicates mean location of AR when reaching the coast.

For AR analysis we use vertical profiles of specific humidity (q, kg kg^{-1}), temperature (T, K), and horizontal wind components (u and v, m s^{-1}) at pressure (p, Pa) levels from 900 to 300 hPa to calculate integrated water vapor (IWV, cm), saturated IWV (IWV_{sat}, cm), and total moisture transport (MT, kg m^{-1} s^{-1}):

$$\mathrm{IWV} = \frac{100}{\rho}\int_{900\,\mathrm{hPa}}^{300\,\mathrm{hPa}} q\,\mathrm{d}p, \tag{1}$$

$$\mathrm{IWV_{sat}} = \frac{100}{\rho}\int_{900\,\mathrm{hPa}}^{300\,\mathrm{hPa}} q_s(T)\,\mathrm{d}p, \tag{2}$$

$$\mathrm{MT} = \frac{1}{g}\left(\int_{900\,\mathrm{hPa}}^{300\,\mathrm{hPa}} qu\,\mathrm{d}p + \int_{900\,\mathrm{hPa}}^{300\,\mathrm{hPa}} qv\,\mathrm{d}p\right). \tag{3}$$

Here q_s is the saturation specific humidity for corresponding T at each p level according to Clausius-Clapeyron relation, ρ is liquid water density, and g is gravitational acceleration. In addition, the ERA-I reanalysis is used to calculate monthly mean meridional moisture flux averaged over 55°S–72°S, 20°W–90°E sector by integrating the meridional component of MT across the total column of the troposphere (following *Tsukernik and Lynch* [2013]). The seasonal cycle is removed from the data prior to calculating the meridional MT.

Snowfall rate is estimated using Micro Rain Radar 2 (MRR) measurements—vertically profiling 24 GHz precipitation radar operating at PE since January 2010 (the only precipitation radar currently operating over the Antarctic ice sheet) [*Gorodetskaya et al.*, 2014]. MRR measurements for the 2009–2012 analysis period are available during 18 January to 31 March 2010, 10 December 2010 to 10 April 2011, and 4 December 2011 to 31 December 2012 (data gaps are due to the power failures at PE). Radar effective reflectivity factor (Z_e, mm^6 m^{-3}) vertical profiles at 1 min resolution are derived from raw MRR measurements of spectral signal power per range based on the algorithm by *Maahn and Kollias* [2012] developed specifically for solid precipitation. Daily snowfall rate (*S*, mm w.e.) is calculated as the sum of hourly mean *S* based on Z_e at 400 m above ground level (the lowest useful range of MRR with 100 m range resolution). We applied a range of Z_e-*S* relationships established by *Matrosov* [2007] for dry snow (ranging from $Z_e = 34S^{1.1}$ to $Z_e = 67S^{1.2}$; see Table 1 therein), expected to be most suitable for PE, where snow always forms at temperatures below −8°C.

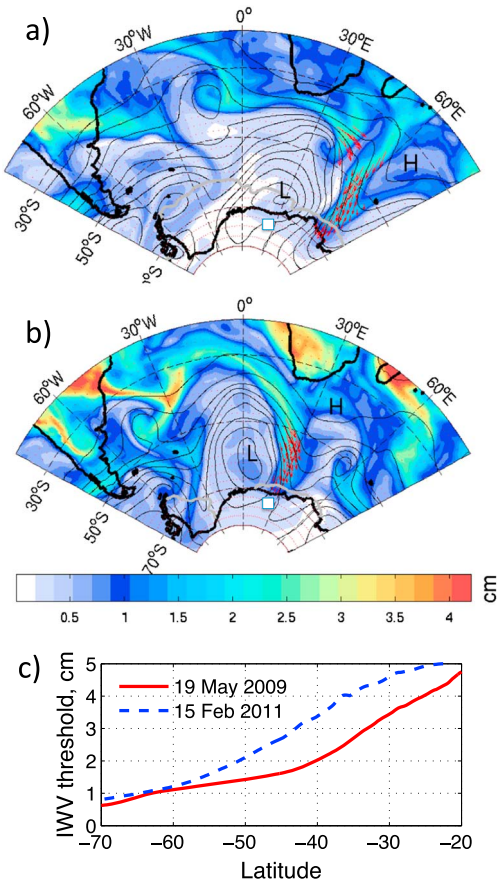

Figure 2. Maps of IWV (cm, equation (1)) at 00 UTC on (a) 19 May 2009 and (b) 15 February 2011. Red arrows indicate vertically integrated total MT (equation (3)) within each AR as identified using the definition adapted for Antarctica (section 3.2). Black contours are 500 hPa geopotential heights, where *L* shows a closed trough at 500 hPa influencing DML and *H* shows the blocking high-pressure ridge downstream of the low. White square shows PE location. (c) IWV threshold as a function of latitude based on equation (4). Based on the ERA-I reanalysis.

3. Results

3.1. Two High-Accumulation Events of 2009 and 2011

Significant contribution to the total local PE SMB during 2009 and 2011 comes from two events—on 18 and 19 May 2009 and 14–16 February 2011. During both events snow height measured by the PE AWS increased by 48–51 mm w.e., thereby contributing a large percentage—up to 21 and 22%—of the total SMB for each year.

Both events were associated with a deep 500 hPa trough, corresponding to a very strong and deep surface cyclone situated north of DML blocked by a high-pressure ridge to its east (Figures 2a and 2b). During the 2009 event, the 500 hPa trough was near 30°E, directing the moisture flux into the ice sheet along 60°E. During the 2011 event, the 500 hPa trough was even more pronounced and was centered near the prime meridian, while directing the moisture flux along 30°E. In both cases, not only the immediate vicinity of PE but also a significant part of DML were characterized by elevated IWV (Figures 2a and 2b). Thus, measurements at PE can be considered representative of a larger area and therefore may reflect the average accumulation over the whole DML region. Similar synoptic patterns with a deep 500 hPa trough and a blocking high-pressure ridge downstream as observed in both 2009 and 2011 are commonly found in midlatitude cases leading to AR formation [*Bao et al.*, 2006].

A large-scale circulation pattern, similar for both cases, steered an intense narrow moisture flux into DML, with the band of enhanced IWV stretching from subtropical latitudes (from the southern Indian Ocean east of Madagascar in 2009 and from the south central Atlantic in 2011) to the East Antarctic ice sheet (Figures 2a and 2b). During the 2011 event the high IWV band reached the coast directly at the longitude of PE, whereas during the 2009 event it reached the coast further east and then continued westward along the escarpment zone bringing elevated IWV to PE from the east (Figures 2a and 2b).

3.2. Redefining the ARs for Antarctica

Long narrow corridors of enhanced IWV as were observed in the two cases above are characteristic of ARs [*Ralph et al.*, 2004, 2006; *Bao et al.*, 2006]. *Zhu and Newell* [1998] identified midlatitude ARs as outstanding total MT compared to the mean zonal value at each latitude organized into filamentary forms with their length several times larger than their width (visible in Figure 1). *Ralph et al.* [2004, 2006] demonstrated that IWV can be used to define AR cases as narrow (≤1000 km in width), elongated (≥2000 km in length) bands of enhanced IWV with IWV values in the along-plume and cross-plume direction exceeding 2 cm. The two Antarctic cases described in the previous section satisfy *Zhu and Newell* [1998] criteria and confine large IWV values to the geometric boundaries defined by *Ralph et al.* [2004, 2006]. However, IWV within these bands decrease below 2 cm approaching Antarctica, while still showing large values compared to zonal means.

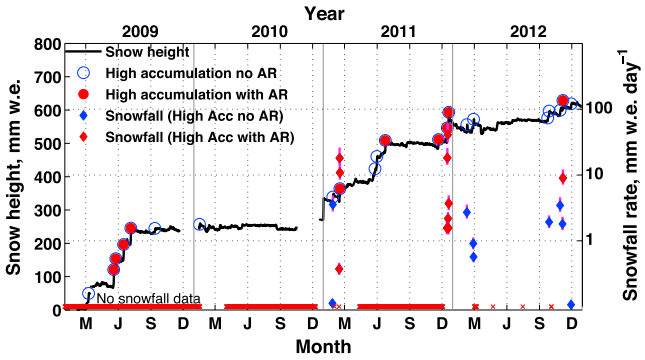

Figure 3. Daily cumulative snow height change and radar-based snowfall rate (*S*) at PE during 2009–2012. High-accumulation events (>10 mm w.e. d^{-1}) are marked with circles: filled red circles for the events associated with ARs (corresponding *S* are shown as red diamonds), and open blue circles for the rest (corresponding *S* are shown as blue diamonds). Vertical magenta line shows uncertainty in *S* depending on different Z_e-*S* relationships [*Matrosov*, 2007]. Note the logarithmic scale for snowfall. Horizontal red bar and crosses at bottom show periods of missing *S* data.

After a detailed study of the presented Antarctic cases on 18 and 19 May 2009 and 14–16 February 2011, we defined a new IWV threshold to identify ARs by taking into account the decreased saturation capacity of the polar troposphere:

$$IWV \geq IWV_{sat,mean} + AR_{coeff}(IWV_{sat,max} - IWV_{sat,mean}), \quad (4)$$

where $IWV_{sat,mean}$ is a zonal mean IWV_{sat} (equation (2)) along each latitude, $IWV_{sat,max}$ is the maximum value of IWV_{sat} along the same latitude, and AR_{coeff} is a coefficient determining relative strength of an AR. After a series of trials, $AR_{coeff} = 0.2$ was found to be the best in identifying all cases when large IWV values were organized into narrow bands reaching the East Antarctic coast. As demonstrated for the two selected cases (Figure 2c), this newly defined IWV threshold satisfies the 2 cm value at 40°–50°S as defined by *Ralph et al.* [2004] for midlatitude ARs but drops to slightly below 1 cm at 70°S near the Antarctic coast. ARs that have the potential to influence DML SMB are identified if IWV exceeds the threshold defined by equation (4) near the Antarctic coast within 20°W–90°E longitudinal sector (coastal latitude varying with longitude), and is present continuously at all latitudes for at least 20° equatorward from the coastal latitude (length > 2000 km), within a limited width of 30° longitude (~1000 km at 70°S increasing equatorward). Such geometric boundaries define the dominant meridional direction of ARs influencing Antarctica. The red arrows in Figures 2a and 2b indicate MT (equation (3)) within the AR boundaries as defined above for the two cases in 2009 and 2011, clearly demonstrating that the large IWV values within the narrow elongated corridor are associated with high poleward MT reaching the coast of the DML.

3.3. High-Accumulation Events and ARs During 2009–2012

AWS measurements of snow accumulation at PE recorded total annual SMB of 230, 23, 227, and 52 mm w.e., during 2009, 2010, 2011, and 2012, respectively. Interannual variability of the PE accumulation is in accordance with the interannual SMB variability over the larger DML region, all featuring the anomalous accumulation during 2009 and 2011 [*Boening et al.*, 2012; *Gorodetskaya et al.*, 2014; *Lenaerts et al.*, 2013]. Large interannual variability in annual SMB at PE is closely related to the number and intensity of high-accumulation events every year (defined as days > 10 mm w. e. d^{-1}; see section 2). Figure 3 shows daily cumulative snow height change at PE during 2009–2012 period with all high-accumulation events marked with circles. Applying the definition of AR adapted for Antarctica to all days during 2009–2012, we found that ARs are responsible for the most extreme among high-accumulation events (with the mean of 22 mm w.e. d^{-1}). Almost all of the AR-associated high-accumulation events occurred during 2009 and 2011.

All high-accumulation events associated with ARs detected during 2009–2012 are listed in Table 1. These events lasted for up to 3 days, and the amount of accumulation and snowfall rates (when available) are given as daily mean value for each event. ARs were detected on specific days during or sometimes the day after these high-accumulation events (Table 1). In the latter case we consider that PE was under the influence of AR development as each AR affects much larger area.

While all high-accumulation events (six in 2009 and eight in 2011) account for almost 100% of the total yearly accumulation, four events associated with ARs in 2009 contribute 74% and five events in 2011 contribute 80% to the total yearly accumulation. In contrast, during 2010 there is only one high-accumulation event detected (not associated with an AR), and during 2012 there are seven high-accumulation events with only one event associated with an AR (with the highest snowfall rate and accumulation of all 2012 events, Figure 3). Radar-based snowfall rate estimates, which only became available in 2010, confirm that

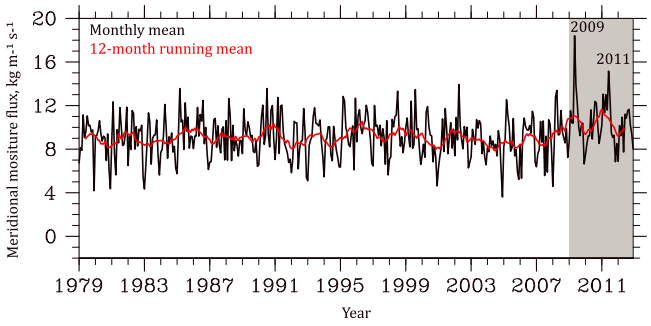

Figure 4. Vertically integrated meridional moisture flux across the 55°–72°S, 20°W–90°E section of the Southern Ocean based on the ERA-I reanalysis for 1979–2012. The seasonal cycle is removed from the data (values are fluctuating around the yearly mean). Gray zone indicates 2009–2012 period of PE data analysis (Figure 3). The year markers show the two largest fluxes during the record in May 2009 and June 2011.

the highest accumulation events are related to intense snowfalls (Table 1 and Figure 3). Thus, the yearly accumulation depends strongly on the number of high-accumulation events and intensity of each particular event. Our results show that anomalously high snow accumulation in 2009 and 2011 can be attributed to a few extreme accumulation events, all of which were associated with ARs reaching Antarctic coast with their core axes within 7°E–60°E (Table 1).

3.4. Poleward Moisture Flux During 1979–2012

To put the recent years with anomalously high accumulation into long-term context, we examined the meridional moisture flux time series averaged monthly over 1979–2012 period and spatially over a sector of the Southern Ocean (55°S–72°S, 20°W–90°E; Figure 4). Poleward MT is primarily associated with synoptic activity; and therefore, it is highly variable on daily, monthly, and interannual time scales. Although DML sector of the Southern Ocean is known for its synoptic activity, it mostly favors zonal transport of cyclones, while meridional propagation of synoptic systems is rare [*Simmonds and Keay*, 2000; *Uotila et al.*, 2013]. Therefore, AR events, as manifestations of poleward MT, can be expected to influence monthly and regionally averaged data. For example, the May 2009 anomaly of the mean integrated meridional moisture flux (18.4 kg m^{-1} s^{-1}, which is about 2 times the mean over the entire period of 9.2 kg m^{-1} s^{-1}), associated with two very high accumulation events produced by ARs, stands out in the 34 year record as unprecedented (Figure 4). The 18–19 May and 25 May 2009 AR events not only were strong enough to dominate over a monthly average, these narrow channeled ARs also managed to dominate meridional MT across a wide longitudinal sector. The monthly peaks of 2011 are less prominent, with the annual maximum flux in June 2011 (15.2 kg m^{-1} s^{-1}) and a secondary maximum in February (13.2 kg m^{-1} s^{-1}). Both of these months in 2011 and May 2009 stand out in Figure 3 as high-accumulation events associated with ARs. Such enhanced poleward moisture fluxes are expected to translate into regional accumulation anomalies, which is consistent with the modeling study of *Lenaerts et al.* [2013], showing positive SMB anomalies in the 10°W–70°E sector.

4. Conclusions and Outlook

Measurements of SMB and snowfall at Princess Elisabeth station, located in the escarpment area of DML, East Antarctica, during 2009–2012 were combined with the ERA-I large-scale meteorological fields, in order to investigate the relationship between atmospheric rivers and high-accumulation events, leading to anomalously high annual accumulation during 2009 and 2011. Two specific cases, each strongly contributing to the total annual accumulation at PE, on 18 and 19 May 2009 and 14–16 February 2011, were analyzed in terms of moisture transport patterns and associated large-scale circulation. Strong moisture fluxes and associated enhanced IWV values were concentrated along a narrow and long corridor directed toward the East Antarctic coast at the eastern flank of a deep cyclone centered north of DML and blocked on the east by a high-pressure ridge. The importance of such blocking events in the heat and moisture transport toward the Antarctic interior was emphasized in earlier studies [e.g., *Hirasawa et al.*, 2000, 2013; *Frezzotti et al.*, 2007]. We show that such synoptic and associated moisture flux patterns of meridional nature are characteristic of ARs and introduce a modified definition for ARs in Antarctica, which considers a lower saturation capacity of the polar troposphere. Applying this definition to the entire period 2009–2012, we find that the anomalously high accumulation observed at PE in 2009 and 2011 can be attributed to a few extreme accumulation events (four to five per year), all of which were associated with ARs reaching the Antarctic coast within the 7°E–60°E longitudinal sector.

Only a subset of the ARs identified within the 20°W–90°E longitudinal sector was associated with high accumulation at PE (in total, there were identified 13, 8, and 3 ARs during 2009, 2011, and 2012, respectively).

The sector within which these ARs reach the East Antarctic coast makes them potentially important for DML SMB, and further analysis using other high-resolution accumulation measurements in DML may show even larger impact of ARs on DML accumulation. The relationship between ARs and high-accumulation events is of great importance for understanding interannual variability and trends of the total Antarctic ice sheet SMB, with implications for future SMB changes and also paleorecord interpretation. The large contribution of ARs to DML SMB implies that the difference in the regional total annual SMB is determined by the frequency of occurrence of ARs. This analysis, indicating the important role of ARs in the Antarctic ice sheet mass balance, suggests that climate models simulating Antarctic SMB require adequate representation of ARs.

Acknowledgments

This work was conducted in support of the HYDRANT project funded by the Belgian Federal Science Policy (BELSPO grant EA/01/04AB). Coauthor M. Tsukernik was supported by NSF grant 1246178. The radar and AWS data at PE are part of the new data set freely available upon request via the project website (http://ees.kuleuven.be/hydrant). ERA-I data are available via the ECMWF data portal (http://www.ecmwf.int/en/forecasts/datasets). Logistical and technical support at PE base was provided by the International Polar Foundation. We thank Alexander Mangold (RMI, Belgium) and Erik Verhagen (IPF) for help with on-site instrument maintenance; Wim Boot and Carleen Reijmer (IMAU, Netherlands) for AWS technical and data support; and METEK engineers for MRR technical support. Raw MRR data were processed by Maximilian Maahn (IGM, University of Cologne, Germany). We thank RCS Group at KUL, Jan Lenaerts (IMAU/KUL), and Gwenael Renard for useful feedback. We thank two anonymous reviewers for constructive comments on the manuscript.

The Editor thanks two anonymous reviewers for their assistance in evaluating this paper.

References

Bao, J.-W., S. A. Michelson, P. J. Neiman, F. M. Ralph, and J. M. Wilczak (2006), Interpretation of enhanced integrated water vapor bands associated with extratropical cyclones: Their formation and connection to tropical moisture, *Mon. Weather Rev.*, *134*(4), 1063–1080, doi:10.1175/MWR3123.1.

Boening, C., M. Lebsock, F. Landerer, and G. Stephens (2012), Snowfall-driven mass change on the East Antarctic ice sheet, *Geophys. Res. Lett.*, *39*(21), L21501, doi:10.1029/2012GL053316.

Braaten, D. A. (2000), Direct measurements of episodic snow accumulation on the Antarctic polar plateau, *J. Geophys. Res.*, *105*(D8), 10,119–10,128, doi:10.1029/2000JD900099.

Bromwich, D. H. (1988), Snowfall in high southern latitudes, *Rev. Geophys.*, *26*(1), 149–168, doi:10.1029/RG026i001p00149.

Dee, D. P., et al. (2011), The ERA-Interim reanalysis: Configuration and performance of the data assimilation system, *Q. J. R. Meteorolog. Soc.*, *137*(656), 553–597, doi:10.1002/qj.828.

Dettinger, M. D., F. M. Ralph, T. Das, P. J. Neiman, and D. R. Cayan (2011), Atmospheric rivers, floods and the water resources of California, *Water*, *3*(4), 445–478, doi:10.3390/w3020445.

Frezzotti, M., S. Urbini, M. Proposito, C. Scarchilli, and S. Gandolfi (2007), Spatial and temporal variability of surface mass balance near Talos Dome, East Antarctica, *J. Geophys. Res.*, *112*(F2), F02032, doi:10.1029/2006JF000638.

Fujita, S., et al. (2011), Spatial and temporal variability of snow accumulation rate on the East Antarctic ice divide between Dome Fuji and EPICA DML, *Cryosphere*, *5*(4), 1057–1081, doi:10.5194/tc-5-1057-2011.

Gorodetskaya, I. V., N. P. M. Van Lipzig, M. R. Van den Broeke, A. Mangold, W. Boot, and C. H. Reijmer (2013), Meteorological regimes and accumulation patterns at Utsteinen, Dronning Maud Land, East Antarctica: Analysis of two contrasting years, *J. Geophys. Res. Atmos.*, *118*(4), 1700–1715, doi:10.1002/jgrd.50177.

Gorodetskaya, I. V., S. Kneifel, M. Maahn, K. Van Tricht, J. H. Schween, S. Crewell, and N. P. M. Van Lipzig (2014), Cloud and precipitation properties from ground-based remote sensing in East Antarctica, *Cryosphere Discuss.*, *8*, 4195–4241, doi:10.5194/tcd-8-4195-2014.

Hirasawa, N., H. Nakamura, and T. Yamanouchi (2000), Abrupt changes in meteorological conditions observed at an inland Antarctic station in association with wintertime blocking, *Geophys. Res. Lett.*, *27*(13), 1911–1914, doi:10.1029/1999GL011039.

Hirasawa, N., H. Nakamura, H. Motoyama, M. Hayashi, and T. Yamanouchi (2013), The role of synoptic-scale features and advection in prolonged warming and generation of different forms of precipitation at Dome Fuji station, Antarctica, following a prominent blocking event, *J. Geophys. Res. Atmos.*, *118*(13), 6916–6928, doi:10.1002/jgrd.50532.

King, M. A., R. J. Bingham, P. Moore, P. L. Whitehouse, M. J. Bentley, and G. A. Milne (2012), Lower satellite-gravimetry estimates of Antarctic sea-level contribution, *Nature*, *491*(7425), 586–589, doi:10.1038/nature11621.

Knippertz, P., H. Wernli, and G. Gläser (2013), A global climatology of tropical moisture exports, *J. Clim.*, *26*(10), 3031–3045, doi:10.1175/JCLI-D-12-00401.1.

Kopparla, P., E. M. Fischer, C. Hannay, and R. Knutti (2013), Improved simulation of extreme precipitation in a high-resolution atmosphere model, *Geophys. Res. Lett.*, *40*(21), 5803–5808, doi:10.1002/2013GL057866.

Lavers, D. A., and G. Villarini (2013), The nexus between atmospheric rivers and extreme precipitation across Europe, *Geophys. Res. Lett.*, *40*(12), 3259–3264, doi:10.1002/grl.50636.

Lavers, D. A., R. P. Allan, E. F. Wood, G. Villarini, D. J. Brayshaw, and A. J. Wade (2011), Winter floods in Britain are connected to atmospheric rivers, *Geophys. Res. Lett.*, *38*(23), L23803, doi:10.1029/2011GL049783.

Lenaerts, J. T. M., E. van Meijgaard, M. R. van den Broeke, S. R. M. Ligtenberg, M. Horwath, and E. Isaksson (2013), Recent snowfall anomalies in Dronning Maud Land, East Antarctica, in a historical and future climate perspective, *Geophys. Res. Lett.*, *40*(11), 2684–2688, doi:10.1002/grl.50559.

Maahn, M., and P. Kollias (2012), Improved Micro Rain Radar snow measurements using Doppler spectra post-processing, *Atmos. Meas. Tech.*, *5*(11), 2661–2673, doi:10.5194/amt-5-2661-2012.

Matrosov, S. Y. (2007), Modeling backscatter properties of snowfall at millimeter wavelengths, *J. Atmos. Sci.*, *64*, 1727–1736, doi:10.1175/JAS3904.1.

McMillan, M., A. Shepherd, A. Sundal, K. Briggs, A. Muir, A. Ridout, A. Hogg, and D. Wingham (2014), Increased ice losses from Antarctica detected by CryoSat-2, *Geophys. Res. Lett.*, *41*(11), 3899–3905, doi:10.1002/2014GL060111.

Neff, W., G. Compo, F. M. Ralph, and M. D. Shupe (2014), Continental heat anomalies and the extreme melting of the Greenland ice surface in 2012 and 1889, *J. Geophys. Res. Atmos.*, *119*, 6520–6536, doi:10.1002/2014JD021470.

Nicolas, J. P., and D. H. Bromwich (2011), Precipitation changes in high southern latitudes from global reanalyses: A cautionary tale, *Surv. Geophys.*, *32*(4–5), 475–494, doi:10.1007/s10712-011-9114-6.

Noone, D., J. Turner, and R. Mulvaney (1999), Atmospheric signals and characteristics of accumulation in Dronning Maud Land, Antarctica, *J. Geophys. Res.*, *104*(D16), 19,191–19,211, doi:10.1029/1999JD900376.

Ralph, F. M., P. J. Neiman, and G. A. Wick (2004), Satellite and CALJET aircraft observations of atmospheric rivers over the Eastern North Pacific Ocean during the winter of 1997/98, *Mon. Weather Rev.*, *132*, 1721–1745, doi:10.1175/1520-0493(2004)132<1721:SACAOO>2.0.CO;2.

Ralph, F. M., P. J. Neiman, G. A. Wick, S. I. Gutman, M. D. Dettinger, D. R. Cayan, and A. B. White (2006), Flooding on California's Russian River: Role of atmospheric rivers, *Geophys. Res. Lett.*, *33*(13), L13801, doi:10.1029/2006GL026689.

Ralph, F. M., P. J. Neiman, G. N. Kiladis, K. Weickmann, and D. W. Reynolds (2011), A multiscale observational case study of a Pacific atmospheric river exhibiting tropical-extratropical connections and a mesoscale frontal wave, *Mon. Weather Rev.*, *139*(4), 1169–1189, doi:10.1175/2010MWR3596.1.

Ralph, F. M., T. Coleman, P. J. Neiman, R. J. Zamora, and M. D. Dettinger (2014), Observed impacts of duration and seasonality of atmospheric-river landfalls on soil moisture and runoff in coastal Northern California, *J. Hydrometeorol.*, *14*, 443–459, doi:10.1175/JHM-D-12-076.1.

Reijmer, C. H., and M. R. van den Broeke (2003), Temporal and spatial variability of the surface mass balance in Dronning Maud Land, Antarctica, as derived from automatic weather stations, *J. Glaciol.*, *49*(167), 512–520, doi:10.3189/172756503781830494.

Rignot, E., J. Mouginot, M. Morlighem, H. Seroussi, and B. Scheuchl (2014), Widespread, rapid grounding line retreat of Pine Island, Thwaites, Smith and Kohler glaciers, West Antarctica from 1992 to 2011, *Geophys. Res. Lett.*, *41*(10), 3502–3509, doi:10.1002/2014GL060140.

Schlosser, E., K. W. Manning, J. G. Powers, M. G. Duda, G. Birnbaum, and K. Fujita (2010), Characteristics of high-precipitation events in Dronning Maud Land, Antarctica, *J. Geophys. Res.*, *115*(D14), D14107, doi:10.1029/2009JD013410.

Shepherd, A., et al. (2012), A reconciled estimate of ice-sheet mass balance, *Science*, *338*(6111), 1183–1189, doi:10.1126/science.1228102.

Simmonds, I., and K. Keay (2000), Mean Southern Hemisphere extratropical cyclone behavior in the 40-year NCEP-NCAR reanalysis, *J. Clim.*, *13*, 873–885, doi:10.1175/1520-0442(2000)013<0873:MSHECB>2.0.CO;2.

Tsukernik, M., and A. H. Lynch (2013), Atmospheric meridional moisture flux over the Southern Ocean: A story of the Amundsen Sea, *J. Clim.*, *26*(20), 8055–8064, doi:10.1175/JCLI-D-12-00381.1.

Uotila, P., T. Vihma, and M. Tsukernik (2013), Close interactions between the Antarctic cyclone budget and large-scale atmospheric circulation, *Geophys. Res. Lett.*, *40*, 3237–3241, doi:10.1002/grl.50560.

Van Lipzig, N. P. M., and M. R. van den Broeke (2002), A model study on the relation between atmospheric boundary-layer dynamics and poleward atmospheric moisture transport in Antarctica, *Tellus A*, *54*(5), 497–511, doi:10.1034/j.1600-0870.2002.201404.x.

Viale, M., and M. N. Nuñez (2011), Climatology of winter orographic precipitation over the subtropical Central Andes and associated synoptic and regional characteristics, *J. Hydrometeorol.*, *12*(4), 481–507, doi:10.1175/2010JHM1284.1.

Wick, G. A., P. J. Neiman, F. M. Ralph, and T. M. Hamill (2013), Evaluation of forecasts of the water vapor signature of atmospheric rivers in operational numerical weather prediction models, *Weather Forecast.*, *28*(6), 1337–1352, doi:10.1175/WAF-D-13-00025.1.

Zhu, Y., and R. E. Newell (1998), A proposed algorithm for moisture fluxes from atmospheric rivers, *Mon. Weather Rev.*, *126*, 725–735, doi:10.1175/1520-0493(1998)126<0725:APAFMF>2.0.CO;2.